



Observation of the semileptonic decay $B^+ \rightarrow p\bar{p}\mu^+\nu_\mu$

LHCb collaboration[†]

Abstract

The Cabibbo-suppressed semileptonic decay $B^+ \rightarrow p\bar{p}\mu^+\nu_\mu$ is observed for the first time using a sample of pp collisions corresponding to an integrated luminosity of 1.0, 2.0 and 1.9 fb⁻¹ at centre-of-mass energies of 7, 8 and 13 TeV, respectively. The differential branching fraction is measured as a function of the $p\bar{p}$ invariant mass. The total branching fraction is measured to be

$$\mathcal{B}(B^+ \rightarrow p\bar{p}\mu^+\nu_\mu) = (5.27_{-0.24}^{+0.23} \pm 0.21 \pm 0.15) \times 10^{-6},$$

where the first uncertainty is statistical, the second systematic and the third is from the uncertainty on the normalisation branching fraction.

For submission to JHEP

© 2019 CERN for the benefit of the LHCb collaboration. CC-BY-4.0 licence.

[†]Authors are listed at the end of this paper.

1 Introduction

Studies of semileptonic B meson decays have recently generated interest due to a number of anomalous results. Measurements of the observables $R(D)$ and $R(D^*)$ [1–6] have shown hints of lepton non-universality with a combined significance of over 3σ [7]. To probe the flavour structure of any possible new physics contributions to these results, it is desirable to make analogous measurements for decays involving different quark transitions, for example $b \rightarrow u$. To that end, the mode $B^+ \rightarrow p\bar{p}l^+\nu_l$ is promising experimentally, particularly when performing the measurement at a hadron collider, as the requirement of a proton anti-proton pair in the final state should significantly reduce combinatorial background. Semileptonic decays of B mesons to a final state containing multiple baryons are as yet unobserved, although the Belle collaboration has found evidence for $B^+ \rightarrow p\bar{p}e^+\nu_e$ with 3.2σ significance. They measured the branching fraction to be $(8.2^{+3.7}_{-3.2} \pm 0.6) \times 10^{-6}$ [8].

A theoretical model of $B^+ \rightarrow p\bar{p}\mu^+\nu_\mu$ has been constructed with perturbative QCD (pQCD) [9]. This model is based on studies of several similar fully hadronic $B \rightarrow Y\bar{Y}'X$ decays where Y represents a baryon and X one or more mesons. By fitting the angular distributions and decay rates of the hadronic modes [10, 11] the authors of these papers estimate the total branching fraction and the differential decay rate of $B^+ \rightarrow p\bar{p}\mu^+\nu_\mu$. However, the predicted branching fraction is two orders of magnitude larger than the Belle measurement of $B^+ \rightarrow p\bar{p}l^+\nu_l$.

The measurements of the fully hadronic modes show some features that merit further investigation. It is surprising that the branching fractions of decays of B mesons to final states comprising only two baryons are suppressed compared to those of two baryons and one or more extra final state particles [12]. For example the branching fraction of $B^0 \rightarrow p\bar{p}$ is two orders of magnitude smaller than that of the similar decay $B^0 \rightarrow p\bar{p}\pi^+\pi^-$ [12, 13]. Furthermore, the invariant mass distributions of the baryon pair in $B \rightarrow Y\bar{Y}'X$ decays show the so-called threshold enhancement effect. This is a characteristic shape that peaks at low values [14–17]. Understanding the dynamics that leads to such features is difficult in fully hadronic decays, due to the interaction of the two baryons and the extra hadrons. It is therefore desirable to study semileptonic decays, such as $B^+ \rightarrow p\bar{p}\mu^+\nu_\mu$, where such final-state interactions are absent.

In this paper, the first observation of the decay $B^+ \rightarrow p\bar{p}\mu^+\nu_\mu$ is presented. As the dynamics of the transition are not known, the branching fraction is measured in bins of $p\bar{p}$ invariant mass. These bins are then summed to obtain a measurement of the total branching fraction. The decay $B^+ \rightarrow J/\psi K^+$, with $J/\psi \rightarrow \mu^+\mu^-$ is chosen as the normalisation mode as it is fully reconstructed and can pass similar selection requirements to the signal. The branching fraction within a bin i is

$$d\mathcal{B}(B^+ \rightarrow p\bar{p}\mu^+\nu_\mu)_i = \frac{N(B^+ \rightarrow p\bar{p}\mu^+\nu_\mu)_i}{N(B^+ \rightarrow (J/\psi \rightarrow \mu^+\mu^-)K^+)} \times \frac{\epsilon(B^+ \rightarrow (J/\psi \rightarrow \mu^+\mu^-)K^+)}{\epsilon(B^+ \rightarrow p\bar{p}\mu^+\nu_\mu)_i} \times \mathcal{B}(B^+ \rightarrow (J/\psi \rightarrow \mu^+\mu^-)K^+), \quad (1)$$

where $N(B^+ \rightarrow p\bar{p}\mu^+\nu_\mu)_i$ is the yield of $B^+ \rightarrow p\bar{p}\mu^+\nu_\mu$ candidates in bin i , $N(B^+ \rightarrow (J/\psi \rightarrow \mu^+\mu^-)K^+)$ is the total yield of $B^+ \rightarrow J/\psi K^+$ candidates and ϵ represents the detector acceptance as well as the reconstruction and selection efficiencies of the two modes. The branching fractions of $B^+ \rightarrow J/\psi K^+$ and $J/\psi \rightarrow \mu^+\mu^-$ decays are taken from Ref. [12].

42 The signal yields are extracted from fits to a variable called the corrected mass, which
 43 accounts for the unreconstructed neutrino in the signal decay. It is defined by [18]

$$m_{\text{corr}} = |p'_T| + \sqrt{|p'_T|^2 + m_{\text{vis}}^2}, \quad (2)$$

44 where $|p'_T|$ is defined as the magnitude of the reconstructed $p\bar{p}\mu^+$ momentum transverse
 45 to the B flight direction and m_{vis}^2 is the square of the $p\bar{p}\mu^+$ invariant mass.

46 This study uses the data collected by the LHCb detector in proton-proton collisions in
 47 2011, 2012 and 2016. This corresponds to integrated luminosities of 1.0, 2.0 and 1.9 fb⁻¹
 48 at centre-of-mass energies of 7, 8 and 13 TeV, respectively. The 2011 and 2012 data sets
 49 are treated together and collectively referred to by the sobriquet Run 1. Charge conjugate
 50 processes are implied throughout this paper.

51 2 Detector and simulation

52 The LHCb detector [19, 20] is a single-arm forward spectrometer covering the
 53 pseudorapidity range $2 < \eta < 5$, designed for the study of particles containing b or
 54 c quarks. The detector includes a high-precision tracking system consisting of a silicon-
 55 strip vertex detector surrounding the pp interaction region [21], a large-area silicon-strip
 56 detector located upstream of a dipole magnet with a bending power of about 4 Tm, and
 57 three stations of silicon-strip detectors and straw drift tubes [22, 23] placed downstream
 58 of the magnet. The tracking system provides a measurement of the momentum, p , of
 59 charged particles with a relative uncertainty that varies from 0.5% at low momentum
 60 to 1.0% at 200 GeV/ c . The minimum distance of a track to a primary vertex (PV), the
 61 impact parameter (IP), is measured with a resolution of $(15 + 29/p_T) \mu\text{m}$, where p_T is
 62 the component of the momentum transverse to the beam in GeV/ c . Different types of
 63 charged hadrons are distinguished using information from two ring-imaging Cherenkov
 64 (RICH) detectors [24]. Photons, electrons and hadrons are identified by a calorimeter
 65 system consisting of scintillating-pad and preshower detectors, an electromagnetic and a
 66 hadronic calorimeter. Muons are identified by a system composed of alternating layers of
 67 iron and multiwire proportional chambers [25].

68 The online event selection is performed by a trigger [26], which consists of a hardware
 69 stage that performs some basic selection, followed by a software stage, which applies a
 70 full event reconstruction. At the first level, a track consistent with being a muon with
 71 significant p_T is required to be present in the event. Subsequently in the software stage,
 72 two tracks are required to form a secondary vertex with significant displacement from a
 73 pp interaction vertex. A multivariate algorithm [27] is used to identify vertices that are
 74 consistent with the decay of a b hadron.

75 Simulation is used to determine the efficiency of the signal mode and estimate the shapes
 76 of the signal and several backgrounds modes in the signal m_{corr} fits. In the simulation,
 77 pp collisions are generated using PYTHIA [28] with a specific LHCb configuration [29].
 78 Decays of unstable particles are described by EVTGEN [30], in which final-state radiation
 79 is generated using PHOTOS [31]. The interaction of the generated particles with the
 80 detector, and its response, are implemented using the GEANT4 toolkit [32], as described
 81 in Ref. [33]. The generated B meson p and p_T spectra are corrected to match the data
 82 distributions. A boosted decision tree (BDT) reweighter [34] is trained on samples of

83 $B^+ \rightarrow J/\psi K^+$ data and simulation, independent of those used for the normalisation of the
 84 branching fraction. This is then used to correct all of the simulation used in the analysis.

85 3 Selection

86 Signal candidates are constructed from three tracks which are required to be of good
 87 quality and have a large IP with respect to any PV. The tracks must also have particle
 88 identification criteria consistent with their particle hypothesis. The requirement for
 89 positive proton identification in turn enforces a minimum p of 18 GeV/ c such that they
 90 are above the threshold for radiating in the RICH. Similarly, the muons must have p
 91 above 3 GeV/ c to propagate through the muon stations. All the daughter tracks must
 92 have p_T larger than 1.5 GeV/ c . Finally, the three tracks must form a good quality vertex
 93 significantly displaced from the PV with which the candidate is associated. The signal
 94 muon must have fired the hardware trigger and subsequently the reconstructed candidate
 95 itself must be consistent with the object that fired the software trigger. Potential decays
 96 of η_c , J/ψ and $\psi(2S)$ to $p\bar{p}$ are vetoed with cuts on the $p\bar{p}$ invariant mass of ± 50 MeV
 97 around the respective PDG average masses [12].

98 The selection of the $B^+ \rightarrow (J/\psi \rightarrow \mu^+\mu^-)K^+$ normalisation mode is aligned with that
 99 of the signal to reduce systematic uncertainties. The cuts on the signal protons are
 100 applied to the K^+ and the muon of opposite sign (μ^-), with the exception of the particle
 101 identification criteria. The remaining muon has the signal muon selection applied to it.

102 Further selection is used to reduce several sources of backgrounds relative to the
 103 signal. The largest contribution comes from a melange of partially reconstructed decays
 104 producing two protons and a muon in the final state. It is expected that the largest
 105 among these originates in $b \rightarrow c$ transitions. The most pernicious is $B \rightarrow \bar{A}_c^- p \mu^+ \nu_\mu X$,
 106 where X represents any number of charged or neutral pions (including none) and the \bar{A}_c^-
 107 decays to a final state including one proton. The other major background arises from
 108 $B \rightarrow p\bar{p}DX$ decays, where the D meson may be of any variety (D^0 , D^+ , D^{*+} , *etc.*) but
 109 ultimately decays to a final state with a muon. The contribution of $B \rightarrow p\bar{A}_c^- X$ with
 110 the \bar{A}_c^- decaying semileptonically is comparatively small, as the semileptonic branching
 111 fraction is dominated by $\bar{A}_c^- \rightarrow \Lambda^- \bar{\nu}_l$ decays. The Λ flies a sufficient distance within the
 112 detector before decaying such that the resulting proton is not associated with the B decay
 113 vertex. Another source of partially reconstructed background is formed of $B \rightarrow p\bar{p}\mu^+\nu_\mu X$
 114 decays, where X denotes one or more charged or neutral pions. These decays may proceed
 115 with intermediate N^* or Δ resonances and could naively be expected to have similar
 116 branching fractions to the signal.

117 If any of these partially reconstructed decay modes produces a surplus charged track,
 118 it can be efficiently dealt with by an isolation technique. Once a signal candidate has
 119 been constructed, the other tracks in the event close to the B decay vertex are examined.
 120 A BDT is used to give a probability that these nearby tracks can be associated with
 121 the signal candidate decay-vertex. If the candidate is truly signal, there should be few
 122 other tracks that can be associated with it and the BDT should classify them with a low
 123 probability. On the other hand, the extra track(s) from a partially reconstructed decay
 124 will give a high probability of association if such tracks are found. The isolation algorithm
 125 returns the BDT probabilities for the four tracks most likely to have come from the B
 126 vertex. These four probabilities are themselves combined into a single BDT classifier,

127 known as the charged-isolation BDT. This BDT is trained on simulation to discriminate
 128 signal from $B^+ \rightarrow \bar{\Lambda}_c^- p \mu^+ \nu_\mu$, which is expected to be the largest decay mode with extra
 129 charged tracks. The efficacy of this BDT in reducing such background is shown in Fig. 1.

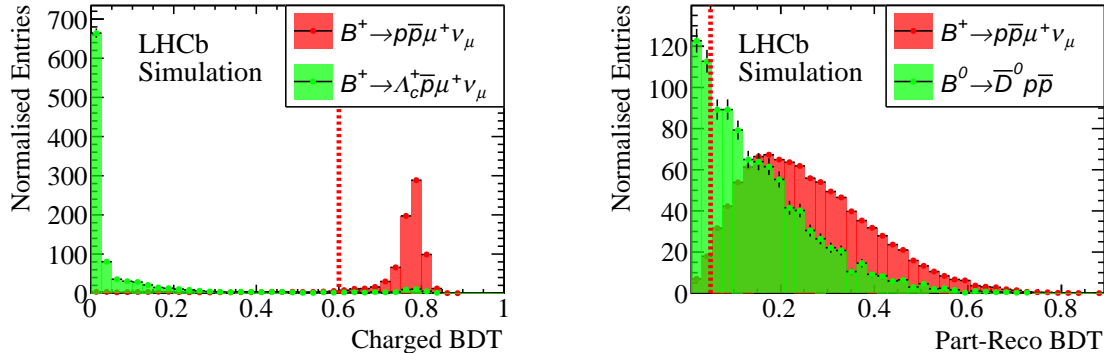


Figure 1: The result of training the (left) charged-isolation BDT and the (right) part-reco BDT. The chosen cut values are indicated by the red line. For some events there are no additional tracks near the B -decay vertex; these events are accepted and do not appear in the charged BDT output. The background samples are chosen such that the Λ_c^+ and \bar{D}^0 decay via $\Lambda_c^+ \rightarrow p K^+ \pi^-$ and $\bar{D}^0 \rightarrow \mu^+ X$.

130 For those partially reconstructed final states with only extraneous neutral particles,
 131 additional suppression is achieved by considering the kinematics of the decays. A further
 132 BDT, the so called part-reco BDT, considers 11 variables: the impact parameter signif-
 133 icance of the three daughter tracks, the $p\bar{p}$ pair and the B^+ candidate with respect to
 134 the PV; the impact parameters of the tracks with respect to the fitted B^+ decay vertex;
 135 the χ^2 of the B^+ vertex fit; the angle between the B^+ candidate momentum and flight
 136 distance vectors; and the difference between the p and \bar{p} momenta. The part-reco BDT is
 137 trained on simulation in order to discriminate signal from a mixture of all the considered
 138 background modes. The result of this training is shown in Fig. 1.

139 An additional background arises from particles that are misidentified as protons
 140 (misID). The particle identification requirements on the proton tracks are therefore further
 141 tightened relative. The background due to the muon being another misidentified particle
 142 is considered and is reduced to a negligible amount with only a loose particle identification
 143 requirement.

144 In addition to the two BDTs and proton identification criteria, one further quantity is
 145 considered: the uncertainty on the corrected mass of the candidate. This is calculated from
 146 the estimated uncertainties on the positions of the B^+ primary and secondary vertices,
 147 and the momenta of the tracks. Selecting lower values of the corrected-mass uncertainty
 148 produces a sharper peak for the signal mode in the corrected mass distribution, which
 149 will aid the discrimination of the signal from background in the fit to determine the yield.
 150 Therefore, in total the selection uses five quantities (two BDTs, the proton PID, the muon
 151 PID and the corrected-mass error). In order to ascertain the optimal cut point, a five
 152 dimensional grid search is performed using pseudoexperiments. Data sets are generated
 153 from the simulation samples with the expected proportions of each background. The
 154 expected signal amount is taken from the central value of the $B^+ \rightarrow p\bar{p}e^+\nu_e$ branching
 155 fraction reported by Belle [8]. For the backgrounds, the current averages for the branching

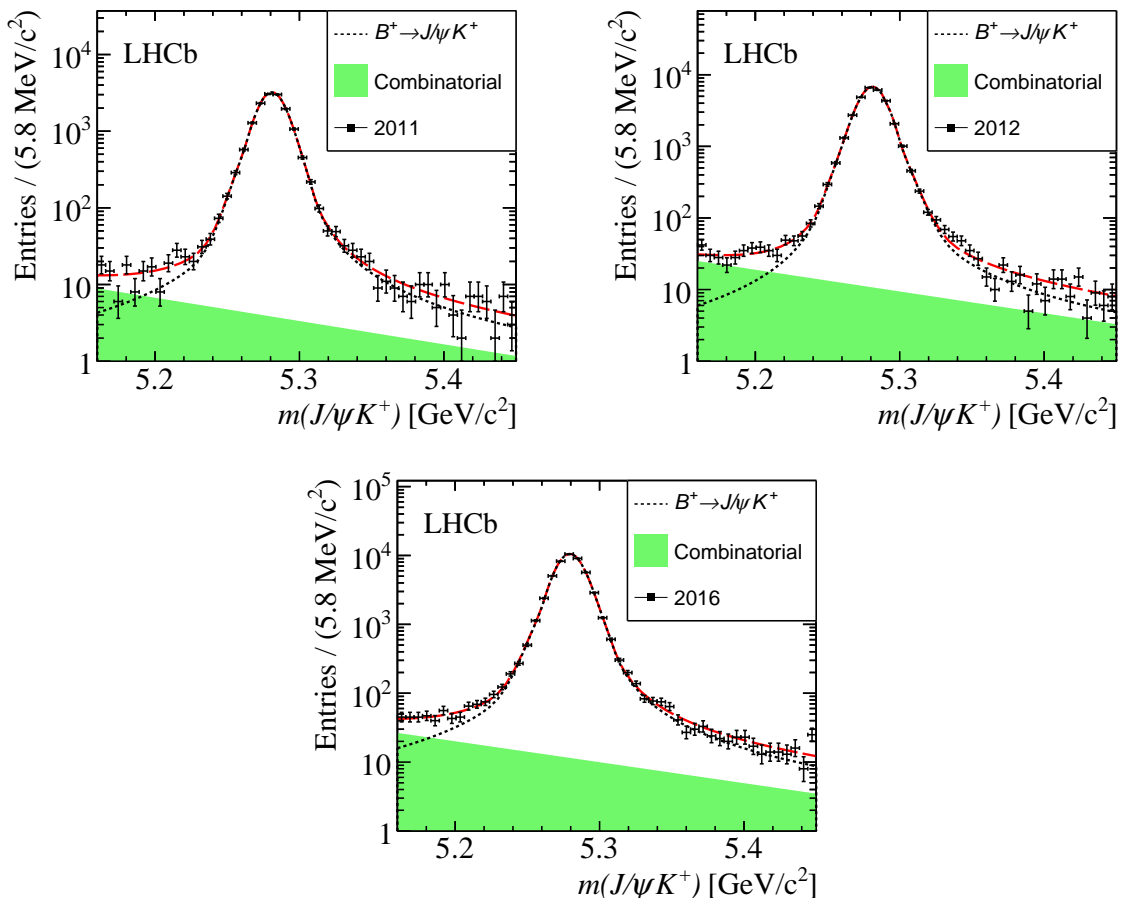


Figure 2: The $m(J/\psi K^+)$ distribution with the fit result shown for the (top left) 2011 data, (top right) 2012 and (bottom) 2016.

156 fractions are used if they have been measured. For those backgrounds that have not been
 157 measured, their branching fractions are estimated relative to that expected for the signal,
 158 accounting for different CKM factors and the available phase space. For each set of cuts
 159 in the grid, the selection is applied to the simulation to estimate the efficiency for each
 160 component. The efficiency of the PID cuts on the simulation is estimated with a data
 161 driven method [35]. A data set is generated in the m_{corr} variable and the expected relative
 162 uncertainty on the signal yield is found by a fit to the simulated data. These fits are not
 163 binned in $m(p\bar{p})$ but take the entire sample together. The set of cuts that produces the
 164 smallest relative uncertainty on the signal yield is chosen.

165 4 Signal and normalisation yields

166 The yields of the signal and normalisation modes are ascertained with unbinned extended
 167 maximum-likelihood fits. In the case of the normalisation mode, the invariant mass
 168 distribution of the $J/\psi K^+$ candidates is fitted. The 2011, 2012 and 2016 data sets are
 169 fitted separately and then the yields combined. These fits are shown in Fig. 2.

170 For the signal mode, the corrected mass is fitted. The distribution of this variable peaks
 171 at the true B^+ rest mass for candidates where one massless particle is not reconstructed.

172 On the other hand, candidates from partially reconstructed decays that are missing one or
 173 more massive particles in addition to the neutrino have wide distributions concentrated at
 174 lower corrected mass values. The Run 1 and 2016 data are combined and fitted together.

175 For the signal component and contributions from partially reconstructed decays, the
 176 shapes are determined using simulation. The shape of the proton misID comes from a
 177 separate independent data sample in which the particle identification requirements on one
 178 of the protons have been removed. Using this data sample, the expected number of the
 179 proton misID candidates can be estimated and a Gaussian constraint is applied to the
 180 yield in the fit. A final background component due to random combinations of protons
 181 and muons, referred to as the combinatorial background, is included in the fit. A sample of
 182 data for which the B^+ decay vertex quality selection has been reversed is used to estimate
 183 the shape of this background. The shape of the signal probability density function (PDF)
 184 is parameterised by the sum of four bifurcated Gaussian functions with a shared mean.
 185 All of the background PDFs are accounted for with kernel density estimation [36].

186 The yields of the signal, proton misID, combinatorial and total partially reconstructed
 187 decays are determined by the fit, as are the relative fractions of each partially reconstructed
 188 mode. All of the fit parameters are free with the exception of the misID yield which is
 189 constrained.

190 The fit in each $m(p\bar{p})$ bin is performed independently. The m_{corr} distributions in
 191 each bin, and the resulting fits are shown in Fig. 3. In each bin the fits are validated
 192 using pseudo-experiments. An ensemble of 10^5 data sets is generated and fitted with the
 193 component yields taken from the fits to data. Some small biases on the signal yield are
 194 found and these are considered as a source of systematic uncertainty.

195 5 Efficiency

196 The efficiencies for the signal and normalisation modes to be reconstructed and selected
 197 are both assessed with simulation. Further corrections are applied to account for known
 198 differences between data and simulation in the track reconstruction efficiency [37] and
 199 the efficiency of the hardware trigger [38]. The efficiency of the particle identification
 200 requirements on each track is evaluated with data [35] and applied to the simulation.

201 The binning in $m(p\bar{p})$ reduces the dependence on the model of the B^+ decay when
 202 calculating the efficiency of the signal mode. However, as the selection cuts on kinematic
 203 quantities of the candidates, there is still some residual dependence on the physics of the
 204 decay. The simulation is therefore re-weighted to represent the pQCD model of Ref. [9]
 205 as the current best estimate of how the decay proceeds. This weighting corrects the
 206 distribution of the invariant mass of the $\mu^+\nu_\mu$ system. The variation of the parameters of
 207 this model is considered as a source of systematic uncertainty.

208 The ratio of selection efficiencies between the signal and normalisation modes in each
 209 bin of $m(p\bar{p})$ is shown in Table 1. These efficiencies are presented separately for the
 210 Run 1 and 2016. They are combined to form an overall efficiency ratio, accounting for the
 211 difference in sample sizes between Run 1 and 2016. This combination is calculated using
 212 the known B^+ production cross-sections [39] and integrated luminosities of each data set.

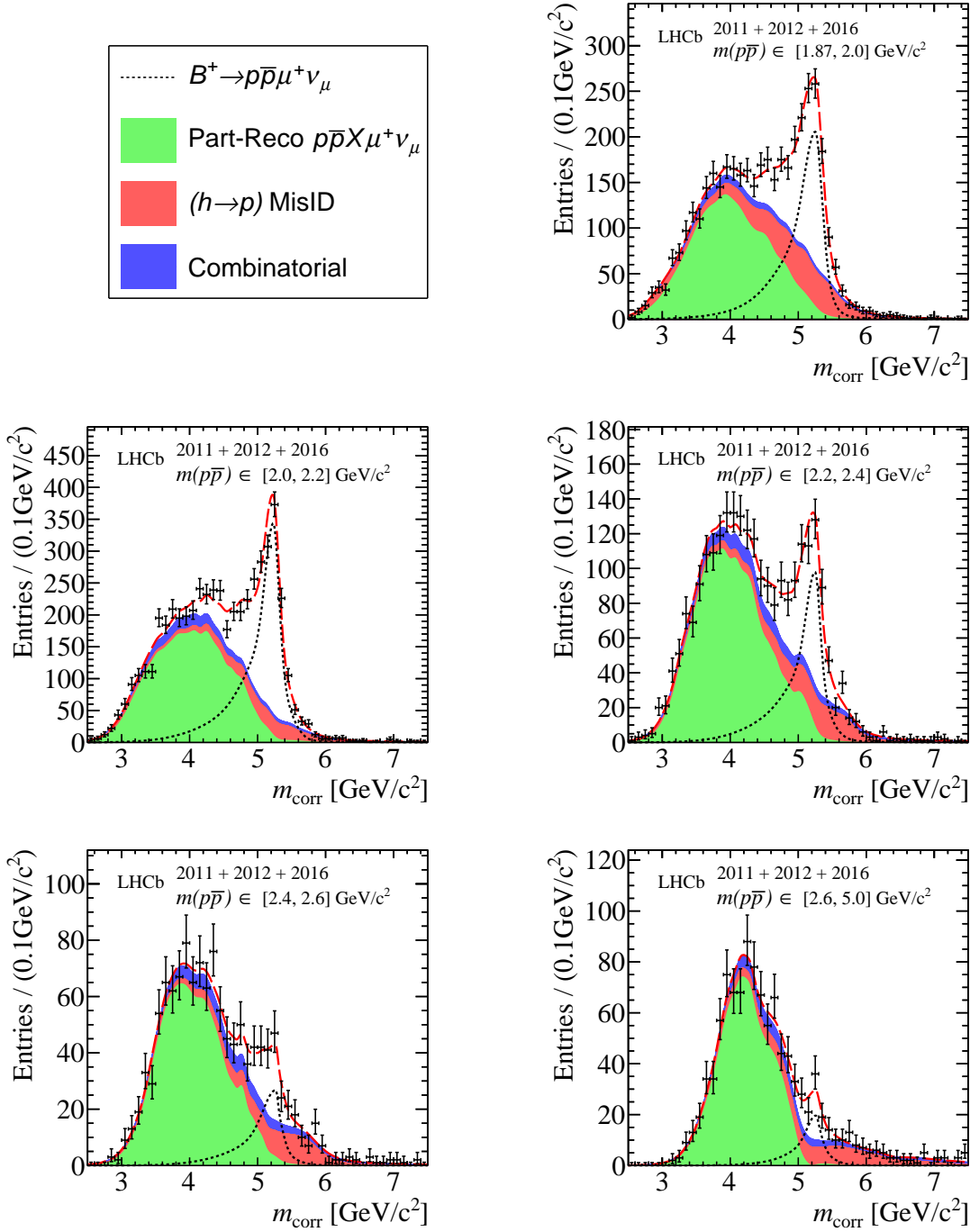


Figure 3: The distributions of m_{corr} in each $m(p\bar{p})$ bin with the fit results shown.

Table 1: The relative efficiencies for Run 1 and 2016 and the weighted combination of both.

$m(p\bar{p})_i$ [GeV/c ²]	$\epsilon(B \rightarrow p\bar{p}\mu\nu)_i/\epsilon(B \rightarrow J/\psi K)$		
	Run 1	2016	Run 1 & 2016
1.87 – 2.0	0.369 ± 0.022	0.567 ± 0.032	0.477 ± 0.024
2.0 – 2.2	0.366 ± 0.020	0.513 ± 0.027	0.446 ± 0.021
2.2 – 2.4	0.358 ± 0.020	0.504 ± 0.026	0.438 ± 0.021
2.4 – 2.6	0.361 ± 0.021	0.519 ± 0.027	0.447 ± 0.021
2.6 – 5.0	0.350 ± 0.020	0.489 ± 0.024	0.426 ± 0.020

6 Systematic uncertainties

The systematic uncertainties can be split into two categories: those that affect the calculation of the ratio of efficiencies of the signal and normalisation modes and those that may change the determination of the signal yield in the fit. For the former, each of the corrections to the simulation contributes a source of uncertainty both from the limited sizes of the samples used to derive the corrections and from the method of deriving them. The parameters of the BDT reweighter used to correct the distributions of p and p_T of the B^+ are altered and the relative efficiencies recalculated. An additional uncertainty due to any residual differences between data and simulation is determined using the $B^+ \rightarrow J/\psi K^+$ mode. The difference in efficiency when cutting on the two BDTs and corrected mass error variable is compared between data and simulation for the mode.

To account for the uncertainty in the correction of the simulation for the reconstruction efficiency of each track, the applied weights are varied within their uncertainties and the relative efficiencies recalculated. Similarly, an uncertainty is assessed for the particle identification weights applied to each track. The uncertainty due to the limited simulation sample sizes used to calculate the efficiencies is also included.

A further uncertainty is due to the physics model that the simulation is weighted to represent. The model affects the kinematic distributions of the daughter tracks which feeds into the efficiency calculation as these distributions are cut on. Due to the unproven nature of the model, a conservative uncertainty is taken. New sets of weights for the simulation are created that sample extreme variations of the model parameters ($\pm 5\sigma$) and for each variation the efficiency is recalculated. Despite this extreme test, the systematic due to the physics model is not dominant, which reflects the flat selection efficiency over the kinematic ranges in which the daughter tracks lie within each bin of $m(p\bar{p})$. Finally, the uncertainties on the B^+ production cross-section [39] and integrated luminosities of the data samples are combined to give the systematic uncertainty on the averaging of the efficiencies when combining Run 1 and 2016.

In the corrected mass fit, uncertainties arise from potential variations in the shapes of the components. This variation is assessed with pseudoexperiments. Data sets are generated with the nominal fit model and then fitted with the nominal model and an alternative. The width of the distribution of differences between the nominal and alternative fits gives the uncertainty. For those components that rely on kernel density estimators, a systematic is assessed for the choice of smoothing parameter by varying it. The uncertainty due to the choice of model for the signal shape is found by replacing the nominal PDF with one constructed with kernel density estimators. The uncertainty due

248 to the limited sizes of the simulation samples is determined by generating new simulation
 249 from the nominal fit PDFs with the same statistics and making alternative PDFs with
 250 those samples. For the shape of the combinatorial background component, an alternative
 251 data sample is trialled which requires the two protons to be of the same charge.

252 A summary of the systematic uncertainties is presented in Table 2. They are given as
 253 relative uncertainties on the branching fraction with the combination accounting for the
 254 correlation of the uncertainties between the two data sets.

Table 2: A summary of the systematic uncertainties on the differential branching fractions. Those pertaining to the efficiency estimate are first with those for the yield extraction below. The particle identification and tracking efficiency uncertainties are assumed to be 100% correlated between Run 1 and 2016.

Source	Relative uncertainties on \mathcal{B} [%]				
	Bin 1	Bin 2	Bin 3	Bin 4	Bin 5
Kinematic reweighting	0.69	0.56	0.39	0.50	0.39
Simulation statistics	3.63	3.18	3.15	3.15	2.98
Tracking efficiency	2.74	2.74	2.74	2.74	2.74
Physics model	0.28	0.57	0.56	0.42	0.32
Particle identification	1.01	0.68	1.30	1.05	1.67
Data-simulation agreement	0.40	0.40	0.40	0.40	0.40
Run 1 and 2016 combination	2.06	1.63	1.65	1.74	1.63
Kernel smoothing	0.02	1.12	2.66	7.91	3.46
Signal model	0.59	2.02	2.97	4.81	9.92
misID model	0.91	0.13	0.56	5.22	13.53
Simulation statistics	0.32	0.02	0.31	2.38	5.18
Combinatorial model	0.90	1.17	1.21	8.51	4.68
Fit bias	0.21	0.13	0.95	2.46	7.84
Total systematic uncertainty	5.33	5.24	6.45	15.58	20.81
Total statistical uncertainty	9.13	5.53	12.47	25.34	29.80

255 7 Results

256 The fitted yields for the signal mode are presented in Table 3. The extracted yields of the
 257 normalisation channel are 14930 ± 260 for 2011, 31380 ± 190 for 2012 and 49270 ± 250 for 2016.
 258 Combining these with the efficiency ratios from Sec. 5, the differential branching fraction
 259 in each $m(p\bar{p})$ bin is calculated relative to the branching fraction of the normalisation
 260 mode. The results are presented in Table 3. The relative differential branching fractions
 261 are summed over the bins, with the correlation of the systematic uncertainties between
 262 the bins accounted for, to give the total relative branching fraction of

$$\frac{\mathcal{B}(B^+ \rightarrow p\bar{p}\mu^+\nu_\mu)}{\mathcal{B}(B^+ \rightarrow (J/\psi \rightarrow \mu^+\mu^-)K^+)} = (8.75 \pm 0.39 \pm 0.35) \times 10^{-2},$$

263 where the first uncertainty is statistical and the second systematic. Multiplying this by
 264 the current average of the normalisation branching fraction [12] leads to

$$\mathcal{B}(B^+ \rightarrow p\bar{p}\mu^+\nu_\mu) = (5.27_{-0.24}^{+0.23} \pm 0.21 \pm 0.15) \times 10^{-6},$$

265 where the third uncertainty is from the normalisation branching fraction. Finally, the
 266 absolute differential branching fraction as a function of $m(p\bar{p})$ is shown in Fig. 4, where
 267 the indicated uncertainties include statistical, systematic and normalisation uncertainty
 268 contributions. As expected from the theory model and the analogous hadronic decays,
 269 the differential distribution peaks at a very low value and falls off sharply. The measured
 270 total branching fraction agrees with the previous measurement from Belle and represents
 271 the first observation of the $B^+ \rightarrow p\bar{p}\mu^+\nu_\mu$ decay mode.

Table 3: The number of observed $B^+ \rightarrow p\bar{p}\mu^+\nu_\mu$ candidates and differential branching fraction in each bin of $m(p\bar{p})$. In the centre column the uncertainties are statistical only. In the right the first uncertainties are statistical, the second systematic and the third from the normalisation branching fractions.

$m(p\bar{p})$ [GeV/c ²]	Signal Yield	$d\mathcal{B}(B^+ \rightarrow p\bar{p}\mu^+\nu_\mu)/dm(p\bar{p})$ [$\times 10^{-6}$ GeV ⁻¹ c ²]
1.87 – 2.0	1208 ⁺¹¹¹ ₋₁₁₀	12.86 ^{+1.18} _{-1.17} \pm 0.69 \pm 0.38
2.0 – 2.2	1826 ⁺⁹⁷ ₋₁₀₅	12.88 ^{+0.69} _{-0.74} \pm 0.68 \pm 0.38
2.2 – 2.4	526 ⁺⁶⁷ ₋₆₄	3.78 ^{+0.48} _{-0.46} \pm 0.24 \pm 0.11
2.4 – 2.6	148 ⁺⁴⁰ ₋₃₅	1.038 ^{+0.279} _{-0.248} \pm 0.162 \pm 0.030
2.6 – 5.0	88 ⁺²⁶ ₋₂₆	0.0542 ^{+0.0163} _{-0.0160} \pm 0.0113 \pm 0.0016

272 Acknowledgements

273 We express our gratitude to our colleagues in the CERN accelerator departments for the
 274 excellent performance of the LHC. We thank the technical and administrative staff at the
 275 LHCb institutes. We acknowledge support from CERN and from the national agencies:
 276 CAPES, CNPq, FAPERJ and FINEP (Brazil); MOST and NSFC (China); CNRS/IN2P3
 277 (France); BMBF, DFG and MPG (Germany); INFN (Italy); NWO (Netherlands); MNiSW
 278 and NCN (Poland); MEN/IFA (Romania); MSHE (Russia); MinECo (Spain); SNSF and
 279 SER (Switzerland); NASU (Ukraine); STFC (United Kingdom); DOE NP and NSF (USA).
 280 We acknowledge the computing resources that are provided by CERN, IN2P3 (France),
 281 KIT and DESY (Germany), INFN (Italy), SURF (Netherlands), PIC (Spain), GridPP
 282 (United Kingdom), RRCKI and Yandex LLC (Russia), CSCS (Switzerland), IFIN-HH
 283 (Romania), CBPF (Brazil), PL-GRID (Poland) and OSC (USA). We are indebted to
 284 the communities behind the multiple open-source software packages on which we depend.
 285 Individual groups or members have received support from AvH Foundation (Germany);
 286 EPLANET, Marie Skłodowska-Curie Actions and ERC (European Union); ANR, Labex
 287 P2IO and OCEVU, and Région Auvergne-Rhône-Alpes (France); Key Research Program
 288 of Frontier Sciences of CAS, CAS PIFI, and the Thousand Talents Program (China);

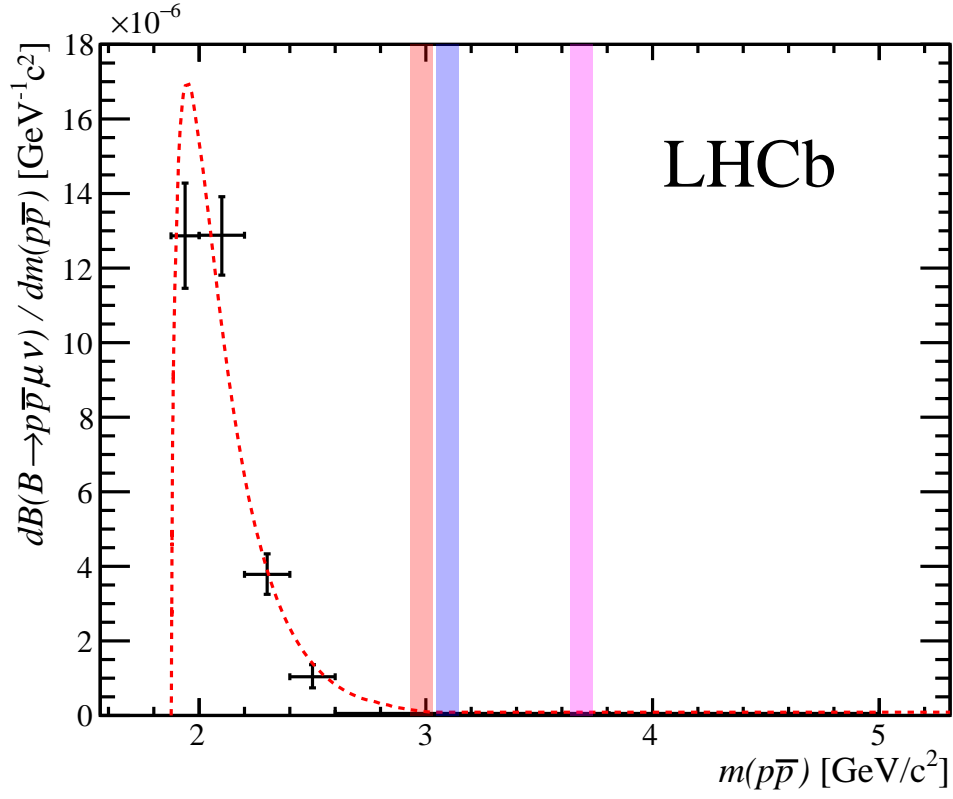


Figure 4: Differential branching fraction as a function of the $p\bar{p}$ invariant mass. The (left) red band indicates the $\eta_c \rightarrow p\bar{p}$ veto and (middle) blue band indicates the $J/\psi \rightarrow p\bar{p}$ veto. The $\psi(2S)$ veto is the (right) pink band. The red dashed line indicates the prediction of the pQCD model normalised to the observed branching fraction [9].

289 RFBR, RSF and Yandex LLC (Russia); GVA, XuntaGal and GENCAT (Spain); the
 290 Royal Society and the Leverhulme Trust (United Kingdom).

8 Supplementary material for LHCb-PAPER-2019-034

Figure 5: The correlations in the uncertainties between bins of $p\bar{p}$ mass.

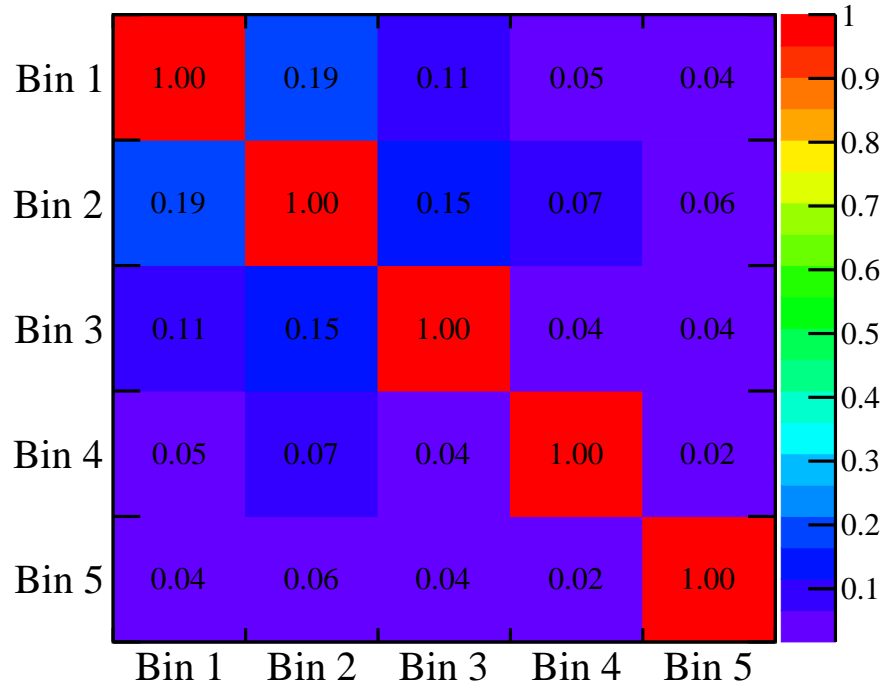


Table 4: The covariance matrix for bins of $m(p\bar{p})$.

$m(p\bar{p})$ [GeV/ c^2]	1.87 – 2.0	2.0 – 2.2	2.2 – 2.4	2.4 – 2.6	2.6 – 5.0
1.87 – 2.0	1.991×10^{-12}	2.800×10^{-13}	8.532×10^{-14}	2.307×10^{-14}	1.249×10^{-15}
2.0 – 2.2	2.800×10^{-13}	1.106×10^{-12}	8.332×10^{-14}	2.264×10^{-14}	1.211×10^{-15}
2.2 – 2.4	8.532×10^{-14}	8.332×10^{-14}	2.945×10^{-13}	6.905×10^{-15}	3.771×10^{-16}
2.4 – 2.6	2.307×10^{-14}	2.264×10^{-14}	6.905×10^{-15}	9.638×10^{-14}	1.011×10^{-16}
2.6 – 5.0	1.249×10^{-15}	1.211×10^{-15}	3.771×10^{-16}	1.011×10^{-16}	3.901×10^{-16}

References

- [1] LHCb collaboration, R. Aaij *et al.*, *Measurement of the ratio of the $\mathcal{B}(B^0 \rightarrow D^{*-}\tau^+\nu_\tau)$ and $\mathcal{B}(B^0 \rightarrow D^{*-}\mu^+\nu_\mu)$ branching fractions using three-prong τ -lepton decays*, Phys. Rev. Lett. **120** (2018) 171802, [arXiv:1708.08856](#).
- [2] LHCb collaboration, R. Aaij *et al.*, *Measurement of the ratio of branching fractions $\mathcal{B}(\bar{B}^0 \rightarrow D^{*+}\tau^-\bar{\nu}_\tau)/\mathcal{B}(\bar{B}^0 \rightarrow D^{*+}\mu^-\bar{\nu}_\mu)$* , Phys. Rev. Lett. **115** (2015) 111803, Publisher's Note *ibid.* **115** (2015) 159901, [arXiv:1506.08614](#).
- [3] Belle collaboration, A. Abdesselam *et al.*, *Measurement of $\mathcal{R}(D)$ and $\mathcal{R}(D^*)$ with a semileptonic tagging method*, [arXiv:1904.08794](#).
- [4] Belle collaboration, S. Hirose *et al.*, *Measurement of the τ lepton polarization and $R(D^*)$ in the decay $\bar{B} \rightarrow D^*\tau^-\bar{\nu}_\tau$* , Phys. Rev. Lett. **118** (2017) 211801, [arXiv:1612.00529](#).
- [5] Belle collaboration, M. Huschle *et al.*, *Measurement of the branching ratio of $\bar{B} \rightarrow D^{(*)}\tau^-\bar{\nu}_\tau$ relative to $\bar{B} \rightarrow D^{(*)}\ell^-\bar{\nu}_\ell$ decays with hadronic tagging at Belle*, Phys. Rev. **D92** (2015) 072014, [arXiv:1507.03233](#).
- [6] BaBar collaboration, J. P. Lees *et al.*, *Evidence for an excess of $\bar{B} \rightarrow D^{(*)}\tau^-\bar{\nu}_\tau$ decays*, Phys. Rev. Lett. **109** (2012) 101802, [arXiv:1205.5442](#).
- [7] Heavy Flavor Averaging Group, Y. Amhis *et al.*, *Averages of b -hadron, c -hadron, and τ -lepton properties as of summer 2016*, Eur. Phys. J. **C77** (2017) 895, [arXiv:1612.07233](#), updated results and plots available at <https://hflav.web.cern.ch>.
- [8] Belle collaboration, K.-J. Tien *et al.*, *Evidence for semileptonic $B^- \rightarrow p\bar{p}\ell^-\bar{\nu}_\ell$ decays*, Phys. Rev. **D89** (2014) 011101, [arXiv:1306.3353](#).
- [9] C. Q. Geng and Y. K. Hsiao, *Semileptonic $B^- \rightarrow p\bar{p}\ell^-\bar{\nu}_\ell$ decays*, Phys. Lett. **B704** (2011) 495, [arXiv:1107.0801](#).
- [10] C. Q. Geng and Y. K. Hsiao, *Angular distributions in three-body baryonic b decays*, Phys. Rev. D **74** (2006) 094023.
- [11] C.-H. Chen, H.-Y. Cheng, C. Q. Geng, and Y. K. Hsiao, *Charmful three-body baryonic b decays*, Phys. Rev. D **78** (2008) 054016.
- [12] Particle Data Group, M. Tanabashi *et al.*, *Review of particle physics*, Phys. Rev. **D98** (2018) 030001.
- [13] LHCb collaboration, R. Aaij *et al.*, *First observation of the rare purely baryonic decay $B^0 \rightarrow p\bar{p}$* , Phys. Rev. Lett. **119** (2017) 232001, [arXiv:1709.01156](#).
- [14] BaBar collaboration, B. Aubert *et al.*, *Evidence for the $B^0 \rightarrow p\bar{p}K^{*0}$ and $B^+ \rightarrow \eta_c K^{*+}$ decays and Study of the Decay Dynamics of B Meson Decays into $p\bar{p}h$ final states*, Phys. Rev. **D76** (2007) 092004, [arXiv:0707.1648](#).

- 329 [15] BaBar collaboration, B. Aubert *et al.*, *Measurements of the Decays $B^0 \rightarrow \bar{D}^0 p\bar{p}$,*
330 *$B^0 \rightarrow \bar{D}^{*0} p\bar{p}$, $B^0 \rightarrow D^- p\bar{p}\pi^+$, and $B^0 \rightarrow D^{*-} p\bar{p}\pi^+$,* Phys. Rev. **D74** (2006) 051101,
331 arXiv:hep-ex/0607039.
- 332 [16] Belle collaboration, M. Z. Wang *et al.*, *Observation of $B^+ \rightarrow p\bar{p}\pi^+$, $B^0 \rightarrow p\bar{p}K^0$, and*
333 *$B^+ \rightarrow p\bar{p}K^{*+}$,* Phys. Rev. Lett. **92** (2004) 131801, arXiv:hep-ex/0310018.
- 334 [17] LHCb, R. Aaij *et al.*, *Evidence for CP Violation in $B^+ \rightarrow p\bar{p}K^+$ Decays,* Phys. Rev.
335 Lett. **113** (2014) 141801, arXiv:1407.5907.
- 336 [18] SLD collaboration, K. Abe *et al.*, *A Measurement of R_b using a vertex mass tag,*
337 Phys. Rev. Lett. **80** (1998) 660, arXiv:hep-ex/9708015.
- 338 [19] LHCb collaboration, A. A. Alves, Jr. *et al.*, *The LHCb Detector at the LHC,* JINST
339 **3** (2008) S08005.
- 340 [20] LHCb collaboration, R. Aaij *et al.*, *LHCb Detector Performance,* Int. J. Mod. Phys.
341 **A30** (2015) 1530022, arXiv:1412.6352.
- 342 [21] R. Aaij *et al.*, *Performance of the LHCb Vertex Locator,* JINST **9** (2014) P09007,
343 arXiv:1405.7808.
- 344 [22] LHCb Outer Tracker Group, R. Arink *et al.*, *Performance of the LHCb Outer Tracker,*
345 JINST **9** (2014) P01002, arXiv:1311.3893.
- 346 [23] LHCb Outer Tracker Group, P. d'Argent *et al.*, *Improved performance of the LHCb*
347 *Outer Tracker in LHC Run 2,* JINST **12** (2017) P11016, arXiv:1708.00819.
- 348 [24] LHCb RICH Group, M. Adinolfi *et al.*, *Performance of the LHCb RICH detector at*
349 *the LHC,* Eur. Phys. J. **C73** (2013) 2431, arXiv:1211.6759.
- 350 [25] A. A. Alves, Jr. *et al.*, *Performance of the LHCb muon system,* JINST **8** (2013)
351 P02022, arXiv:1211.1346.
- 352 [26] R. Aaij *et al.*, *The LHCb Trigger and its Performance in 2011,* JINST **8** (2013)
353 P04022, arXiv:1211.3055.
- 354 [27] V. V. Gligorov and M. Williams, *Efficient, reliable and fast high-level triggering using*
355 *a bonsai boosted decision tree,* JINST **8** (2013) P02013, arXiv:1210.6861.
- 356 [28] T. Sjöstrand, S. Mrenna, and P. Skands, *PYTHIA 6.4 physics and manual,* JHEP
357 **05** (2006) 026, arXiv:hep-ph/0603175; T. Sjöstrand, S. Mrenna, and P. Skands,
358 *A brief introduction to PYTHIA 8.1,* Comput. Phys. Commun. **178** (2008) 852,
359 arXiv:0710.3820.
- 360 [29] I. Belyaev *et al.*, *Handling of the generation of primary events in Gauss, the LHCb*
361 *simulation framework,* J. Phys. Conf. Ser. **331** (2011) 032047.
- 362 [30] D. J. Lange, *The EvtGen particle decay simulation package,* Nucl. Instrum. Meth.
363 **A462** (2001) 152.
- 364 [31] P. Golonka and Z. Was, *PHOTOS Monte Carlo: A precision tool for QED corrections*
365 *in Z and W decays,* Eur. Phys. J. **C45** (2006) 97, arXiv:hep-ph/0506026.

- 366 [32] Geant4 collaboration, J. Allison *et al.*, *Geant4 developments and applications*, IEEE
367 Trans. Nucl. Sci. **53** (2006) 270; Geant4 collaboration, S. Agostinelli *et al.*, *Geant4:*
368 *A simulation toolkit*, Nucl. Instrum. Meth. **A506** (2003) 250.
- 369 [33] M. Clemencic *et al.*, *The LHCb simulation application, Gauss: Design, evolution and*
370 *experience*, J. Phys. Conf. Ser. **331** (2011) 032023.
- 371 [34] A. Rogozhnikov, *Reweighting with Boosted Decision Trees*, J. Phys. Conf. Ser. **762**
372 (2016) , [arXiv:1608.05806](https://arxiv.org/abs/1608.05806), https://github.com/arogozhnikov/hep_ml.
- 373 [35] L. Anderlini *et al.*, *The PIDCalib package*, LHCb-PUB-2016-021, 2016.
- 374 [36] K. S. Cranmer, *Kernel estimation in high-energy physics*, Comput. Phys. Commun.
375 **136** (2001) 198, [arXiv:hep-ex/0011057](https://arxiv.org/abs/hep-ex/0011057).
- 376 [37] LHCb collaboration, R. Aaij *et al.*, *Measurement of the track reconstruction efficiency*
377 *at LHCb*, JINST **10** (2015) P02007, [arXiv:1408.1251](https://arxiv.org/abs/1408.1251).
- 378 [38] S. Tolk, J. Albrecht, F. Dettori, and A. Pellegrino, *Data driven trigger efficiency*
379 *determination at LHCb*, LHCb-PUB-2014-039, 2014.
- 380 [39] LHCb, R. Aaij *et al.*, *Measurement of the b-quark production cross-section in 7*
381 *and 13 TeV pp collisions*, Phys. Rev. Lett. **118** (2017) 052002, [arXiv:1612.05140](https://arxiv.org/abs/1612.05140),
382 [Erratum: Phys. Rev. Lett.119,no.16,169901(2017)].

LHCb collaboration

383 R. Aaij³⁰, C. Abellán Beteta⁴⁷, T. Ackernley⁵⁷, B. Adeva⁴⁴, M. Adinolfi⁵¹, H. Afsharnia⁸,
 384 C.A. Aidala⁷⁸, S. Aiola²⁴, Z. Ajaltouni⁸, S. Akar⁶², P. Albicocco²¹, J. Albrecht¹³, F. Alessio⁴⁵,
 385 M. Alexander⁵⁶, A. Alfonso Alberio⁴³, G. Alkhazov³⁶, P. Alvarez Cartelle⁵⁸, A.A. Alves Jr⁴⁴,
 386 S. Amato², Y. Amhis¹⁰, L. An²⁰, L. Anderlini²⁰, G. Andreassi⁴⁶, M. Andreotti¹⁹, F. Archilli¹⁵,
 387 J. Arnau Romeu⁹, A. Artamonov⁴², M. Artuso⁶⁵, K. Arzymatov⁴⁰, E. Aslanides⁹, M. Atzeni⁴⁷,
 388 B. Audurier²⁵, S. Bachmann¹⁵, J.J. Back⁵³, S. Baker⁵⁸, V. Balagura^{10,b}, W. Baldini^{19,45},
 389 A. Baranov⁴⁰, R.J. Barlow⁵⁹, S. Barsuk¹⁰, W. Barter⁵⁸, M. Bartolini^{22,45,h}, F. Baryshnikov⁷⁴,
 390 G. Bassi²⁷, V. Batozskaya³⁴, B. Batsukh⁶⁵, A. Battig¹³, A. Bay⁴⁶, M. Becker¹³, F. Bedeschi²⁷,
 391 I. Bediaga¹, A. Beiter⁶⁵, L.J. Bel³⁰, V. Belavin⁴⁰, S. Belin²⁵, N. Bely⁴, V. Bellec⁴⁶, K. Belous⁴²,
 392 I. Belyaev³⁷, G. Bencivenni²¹, E. Ben-Haim¹¹, S. Benson³⁰, S. Beranek¹², A. Berezhnoy³⁸,
 393 R. Bernet⁴⁷, D. Berninghoff¹⁵, H.C. Bernstein⁶⁵, E. Bertholet¹¹, A. Bertolin²⁶, C. Betancourt⁴⁷,
 394 F. Betti^{18,e}, M.O. Bettler⁵², Ia. Bezshyiko⁴⁷, S. Bhasin⁵¹, J. Bhom³², M.S. Bieker¹³, S. Bifani⁵⁰,
 395 P. Billoir¹¹, A. Bizzeti^{20,u}, M. Bjørn⁶⁰, M.P. Blago⁴⁵, T. Blake⁵³, F. Blanc⁴⁶, S. Blusk⁶⁵,
 396 D. Bobulska⁵⁶, V. Bocci²⁹, O. Boente Garcia⁴⁴, T. Boettcher⁶¹, A. Boldyrev⁷⁵, A. Bondar^{41,x},
 397 N. Bondar³⁶, S. Borghi^{59,45}, M. Borisyak⁴⁰, M. Borsato¹⁵, J.T. Borsuk³², T.J.V. Bowcock⁵⁷,
 398 C. Bozzi¹⁹, M.J. Bradley⁵⁸, S. Braun¹⁵, A. Brea Rodriguez⁴⁴, M. Brodski⁴⁵, J. Brodzicka³²,
 399 A. Brossa Gonzalo⁵³, D. Brundu²⁵, E. Buchanan⁵¹, A. Buonauro⁴⁷, C. Burr⁴⁵, A. Bursche²⁵,
 400 J.S. Butter³⁰, J. Buytaert⁴⁵, W. Byczynski⁴⁵, S. Cadeddu²⁵, H. Cai⁶⁹, R. Calabrese^{19,g},
 401 L. Calero Diaz²¹, S. Cali²¹, R. Calladine⁵⁰, M. Calvi^{23,i}, M. Calvo Gomez^{43,m}, A. Camboni⁴³,
 402 P. Campana²¹, D.H. Campora Perez⁴⁵, L. Capriotti^{18,e}, A. Carbone^{18,e}, G. Carboni²⁸,
 403 R. Cardinale^{22,h}, A. Cardini²⁵, P. Carniti^{23,i}, K. Carvalho Akiba³⁰, A. Casais Vidal⁴⁴,
 404 G. Casse⁵⁷, M. Cattaneo⁴⁵, G. Cavallero⁴⁵, R. Cenci^{27,p}, J. Cerasoli⁹, M.G. Chapman⁵¹,
 405 M. Charles^{11,45}, Ph. Charpentier⁴⁵, G. Chatzikonstantinidis⁵⁰, M. Chefdeville⁷, V. Chekalina⁴⁰,
 406 C. Chen³, S. Chen²⁵, A. Chernov³², S.-G. Chitic⁴⁵, V. Chobanova⁴⁴, M. Chruszcz³²,
 407 A. Chubykin³⁶, P. Ciambone²¹, M.F. Cicala⁵³, X. Cid Vidal⁴⁴, G. Ciezarek⁴⁵, F. Cindolo¹⁸,
 408 P.E.L. Clarke⁵⁵, M. Clemencic⁴⁵, H.V. Cliff⁵², J. Closier⁴⁵, J.L. Cobbedick⁵⁹, V. Coco⁴⁵,
 409 J.A.B. Coelho¹⁰, J. Cogan⁹, E. Cogneras⁸, L. Cojocariu³⁵, P. Collins⁴⁵, T. Colombo⁴⁵,
 410 A. Comerma-Montells¹⁵, A. Contu²⁵, N. Cooke⁵⁰, G. Coombs⁵⁶, S. Coquereau⁴³, G. Corti⁴⁵,
 411 C.M. Costa Sobral⁵³, B. Couturier⁴⁵, D.C. Craik⁶¹, J. Crkovska⁶⁴, A. Crocombe⁵³,
 412 M. Cruz Torres¹, R. Currie⁵⁵, C.L. Da Silva⁶⁴, E. Dall’Occo³⁰, J. Dalseno^{44,51}, C. D’Ambrosio⁴⁵,
 413 A. Danilina³⁷, P. d’Argent¹⁵, A. Davis⁵⁹, O. De Aguiar Francisco⁴⁵, K. De Bruyn⁴⁵,
 414 S. De Capua⁵⁹, M. De Cian⁴⁶, J.M. De Miranda¹, L. De Paula², M. De Serio^{17,d}, P. De Simone²¹,
 415 J.A. de Vries³⁰, C.T. Dean⁶⁴, W. Dean⁷⁸, D. Decamp⁷, L. Del Buono¹¹, B. Delaney⁵²,
 416 H.-P. Dembinski¹⁴, M. Demmer¹³, A. Dendek³³, V. Denysenko⁴⁷, D. Derkach⁷⁵, O. Deschamps⁸,
 417 F. Desse¹⁰, F. Dettori²⁵, B. Dey⁶, A. Di Canto⁴⁵, P. Di Nezza²¹, S. Didenko⁷⁴, H. Dijkstra⁴⁵,
 418 V. Dobishuk⁴⁹, F. Dordei²⁵, M. Dorigo^{27,y}, A.C. dos Reis¹, L. Douglas⁵⁶, A. Dovbnya⁴⁸,
 419 K. Dreimanis⁵⁷, M.W. Dudek³², L. Dufour⁴⁵, G. Dujany¹¹, P. Durante⁴⁵, J.M. Durham⁶⁴,
 420 D. Dutta⁵⁹, R. Dzhelyadin^{42,†}, M. Dziewiecki¹⁵, A. Dziurda³², A. Dzyuba³⁶, S. Easo⁵⁴,
 421 U. Egede⁵⁸, V. Egorychev³⁷, S. Eidelman^{41,x}, S. Eisenhardt⁵⁵, R. Ekelhof¹³, S. Ek-In⁴⁶,
 422 L. Eklund⁵⁶, S. Ely⁶⁵, A. Ene³⁵, S. Escher¹², S. Esen³⁰, T. Evans⁴⁵, A. Falabella¹⁸, J. Fan³,
 423 N. Farley⁵⁰, S. Farry⁵⁷, D. Fazzini¹⁰, M. Féo⁴⁵, P. Fernandez Declara⁴⁵, A. Fernandez Prieto⁴⁴,
 424 F. Ferrari^{18,e}, L. Ferreira Lopes⁴⁶, F. Ferreira Rodrigues², S. Ferreres Sole³⁰, M. Ferrillo⁴⁷,
 425 M. Ferro-Luzzi⁴⁵, S. Filippov³⁹, R.A. Fini¹⁷, M. Fiorini^{19,g}, M. Firlej³³, K.M. Fischer⁶⁰,
 426 C. Fitzpatrick⁴⁵, T. Fiutowski³³, F. Fleuret^{10,b}, M. Fontana⁴⁵, F. Fontanelli^{22,h}, R. Forty⁴⁵,
 427 V. Franco Lima⁵⁷, M. Franco Sevilla⁶³, M. Frank⁴⁵, C. Frei⁴⁵, D.A. Friday⁵⁶, J. Fu^{24,q},
 428 M. Fuehring¹³, W. Funk⁴⁵, E. Gabriel⁵⁵, A. Gallas Torreira⁴⁴, D. Galli^{18,e}, S. Gallorini²⁶,
 429 S. Gambetta⁵⁵, Y. Gan³, M. Gandelman², P. Gandini²⁴, Y. Gao³, L.M. Garcia Martin⁷⁷,
 430 J. García Pardiñas⁴⁷, B. Garcia Plana⁴⁴, F.A. Garcia Rosales¹⁰, J. Garra Tico⁵², L. Garrido⁴³,

431 D. Gascon⁴³, C. Gaspar⁴⁵, D. Gerick¹⁵, E. Gersabeck⁵⁹, M. Gersabeck⁵⁹, T. Gershon⁵³,
 432 D. Gerstel⁹, Ph. Ghez⁷, V. Gibson⁵², A. Gioventù⁴⁴, O.G. Girard⁴⁶, P. Gironella Gironell⁴³,
 433 L. Giubega³⁵, C. Giugliano¹⁹, K. Gizdov⁵⁵, V.V. Gligorov¹¹, C. Göbel⁶⁷, D. Golubkov³⁷,
 434 A. Golutvin^{58,74}, A. Gomes^{1,a}, P. Gorbounov^{37,5}, I.V. Gorelov³⁸, C. Gotti^{23,i}, E. Govorkova³⁰,
 435 J.P. Grabowski¹⁵, R. Graciani Diaz⁴³, T. Grammatico¹¹, L.A. Granado Cardoso⁴⁵,
 436 E. Graugés⁴³, E. Graverini⁴⁶, G. Graziani²⁰, A. Grecu³⁵, R. Greim³⁰, P. Griffith¹⁹, L. Grillo⁵⁹,
 437 L. Gruber⁴⁵, B.R. Gruberg Cazon⁶⁰, C. Gu³, E. Gushchin³⁹, A. Guth¹², Yu. Guz^{42,45}, T. Gys⁴⁵,
 438 T. Hadavizadeh⁶⁰, G. Haefeli⁴⁶, C. Haen⁴⁵, S.C. Haines⁵², P.M. Hamilton⁶³, Q. Han⁶, X. Han¹⁵,
 439 T.H. Hancock⁶⁰, S. Hansmann-Menzemer¹⁵, N. Harnew⁶⁰, T. Harrison⁵⁷, R. Hart³⁰, C. Hasse⁴⁵,
 440 M. Hatch⁴⁵, J. He⁴, M. Hecker⁵⁸, K. Heijhoff³⁰, K. Heinicke¹³, A. Heister¹³, A.M. Hennequin⁴⁵,
 441 K. Hennessy⁵⁷, L. Henry⁷⁷, J. Heuel¹², A. Hicheur⁶⁶, R. Hidalgo Charman⁵⁹, D. Hill⁶⁰,
 442 M. Hilton⁵⁹, P.H. Hopchev⁴⁶, J. Hu¹⁵, W. Hu⁶, W. Huang⁴, W. Hulsbergen³⁰, T. Humair⁵⁸,
 443 R.J. Hunter⁵³, M. Hushchyn⁷⁵, D. Hutchcroft⁵⁷, D. Hynds³⁰, P. Ibis¹³, M. Idzik³³, P. Ilten⁵⁰,
 444 A. Inglessi³⁶, A. Inyakin⁴², K. Ivshin³⁶, R. Jacobsson⁴⁵, S. Jakobsen⁴⁵, J. Jalocha⁶⁰, E. Jans³⁰,
 445 B.K. Jashal⁷⁷, A. Jawahery⁶³, V. Jevtic¹³, F. Jiang³, M. John⁶⁰, D. Johnson⁴⁵, C.R. Jones⁵²,
 446 B. Jost⁴⁵, N. Jurik⁶⁰, S. Kandybei⁴⁸, M. Karacson⁴⁵, J.M. Kariuki⁵¹, N. Kazeev⁷⁵, M. Kecke¹⁵,
 447 F. Keizer^{52,52}, M. Kelsey⁶⁵, M. Kenzie⁵², T. Ketel³¹, B. Khanji⁴⁵, A. Kharisova⁷⁶, K.E. Kim⁶⁵,
 448 T. Kirn¹², V.S. Kirsebom⁴⁶, S. Klaver²¹, K. Klimaszewski³⁴, S. Koliiev⁴⁹, A. Kondybayeva⁷⁴,
 449 A. Konoplyannikov³⁷, P. Kopciwicz³³, R. Kopecna¹⁵, P. Koppenburg³⁰, I. Kostyuk^{30,49},
 450 O. Kot⁴⁹, S. Kotriakhova³⁶, L. Kravchuk³⁹, R.D. Krawczyk⁴⁵, M. Kreps⁵³, F. Kress⁵⁸,
 451 S. Kretzschmar¹², P. Krokovny^{41,x}, W. Krupa³³, W. Krzemien³⁴, W. Kucewicz^{32,l},
 452 M. Kucharczyk³², V. Kudryavtsev^{41,x}, H.S. Kuindersma³⁰, G.J. Kunde⁶⁴, T. Kvaratskheliya³⁷,
 453 D. Lacarrere⁴⁵, G. Lafferty⁵⁹, A. Lai²⁵, D. Lancierini⁴⁷, J.J. Lane⁵⁹, G. Lanfranchi²¹,
 454 C. Langenbruch¹², T. Latham⁵³, F. Lazzari^{27,v}, C. Lazzeroni⁵⁰, R. Le Gac⁹, R. Lefèvre⁸,
 455 A. Leflat³⁸, F. Lemaître⁴⁵, O. Leroy⁹, T. Lesiak³², B. Leverington¹⁵, H. Li⁶⁸, X. Li⁶⁴, Y. Li⁵,
 456 Z. Li⁶⁵, X. Liang⁶⁵, R. Lindner⁴⁵, V. Lisovskyi¹⁰, G. Liu⁶⁸, X. Liu³, D. Loh⁵³, A. Loi²⁵,
 457 J. Lomba Castro⁴⁴, I. Longstaff⁵⁶, J.H. Lopes², G. Loustau⁴⁷, G.H. Lovell⁵², Y. Lu⁵,
 458 D. Lucchesi^{26,o}, M. Lucio Martinez³⁰, Y. Luo³, A. Lupato²⁶, E. Luppi^{19,g}, O. Lupton⁵³,
 459 A. Lusiani²⁷, X. Lyu⁴, S. Maccolini^{18,e}, F. Machefert¹⁰, F. Maciuc³⁵, V. Macko⁴⁶,
 460 P. Mackowiak¹³, S. Maddrell-Mander⁵¹, L.R. Madhan Mohan⁵¹, O. Maev^{36,45}, A. Maevskiy⁷⁵,
 461 D. Maisuzenko³⁶, M.W. Majewski³³, S. Malde⁶⁰, B. Malecki⁴⁵, A. Malinin⁷³, T. Maltsev^{41,x},
 462 H. Malygina¹⁵, G. Manca^{25,f}, G. Mancinelli⁹, R. Manera Escalero⁴³, D. Manuzzi^{18,e},
 463 D. Marangotto^{24,q}, J. Maratas^{8,w}, J.F. Marchand⁷, U. Marconi¹⁸, S. Mariani²⁰,
 464 C. Marin Benito¹⁰, M. Marinangeli⁴⁶, P. Marino⁴⁶, J. Marks¹⁵, P.J. Marshall⁵⁷, G. Martellotti²⁹,
 465 L. Martinazzoli⁴⁵, M. Martinelli²³, D. Martinez Santos⁴⁴, F. Martinez Vidal⁷⁷, A. Massafferri¹,
 466 M. Materok¹², R. Matev⁴⁵, A. Mathad⁴⁷, Z. Mathe⁴⁵, V. Matiunin³⁷, C. Matteuzzi²³,
 467 K.R. Mattioli⁷⁸, A. Mauri⁴⁷, E. Maurice^{10,b}, M. McCann^{58,45}, L. McConnell¹⁶, A. McNab⁵⁹,
 468 R. McNulty¹⁶, J.V. Mead⁵⁷, B. Meadows⁶², C. Meaux⁹, G. Meier¹³, N. Meinert⁷¹,
 469 D. Melnychuk³⁴, S. Meloni^{23,i}, M. Merk³⁰, A. Merli²⁴, M. Mikhasenko⁴⁵, D.A. Milanese⁷⁰,
 470 E. Millard⁵³, M.-N. Minard⁷, O. Mineev³⁷, L. Minzoni^{19,g}, S.E. Mitchell⁵⁵, B. Mitreska⁵⁹,
 471 D.S. Mitzel⁴⁵, A. Mödden¹³, A. Mogini¹¹, R.D. Moise⁵⁸, T. Mombächer¹³, I.A. Monroy⁷⁰,
 472 S. Monteil⁸, M. Morandin²⁶, G. Morello²¹, M.J. Morello^{27,t}, J. Moron³³, A.B. Morris⁹,
 473 A.G. Morris⁵³, R. Mountain⁶⁵, H. Mu³, F. Muheim⁵⁵, M. Mukherjee⁶, M. Mulder³⁰, D. Müller⁴⁵,
 474 K. Müller⁴⁷, V. Müller¹³, C.H. Murphy⁶⁰, D. Murray⁵⁹, P. Muzzetto²⁵, P. Naik⁵¹, T. Nakada⁴⁶,
 475 R. Nandakumar⁵⁴, A. Nandi⁶⁰, T. Nanut⁴⁶, I. Nasteva², M. Needham⁵⁵, N. Neri^{24,q},
 476 S. Neubert¹⁵, N. Neufeld⁴⁵, R. Newcombe⁵⁸, T.D. Nguyen⁴⁶, C. Nguyen-Mau^{46,n}, E.M. Niel¹⁰,
 477 S. Nieswand¹², N. Nikitin³⁸, N.S. Nolte⁴⁵, C. Nunez⁷⁸, A. Oblakowska-Mucha³³, V. Obraztsov⁴²,
 478 S. Ogilvy⁵⁶, D.P. O’Hanlon¹⁸, R. Oldeman^{25,f}, C.J.G. Onderwater⁷², J. D. Osborn⁷⁸,
 479 A. Ossowska³², J.M. Otalora Goicochea², T. Ovsiannikova³⁷, P. Owen⁴⁷, A. Oyanguren⁷⁷,
 480 P.R. Pais⁴⁶, T. Pajero^{27,t}, A. Palano¹⁷, M. Palutan²¹, G. Panshin⁷⁶, A. Papanestis⁵⁴,

481 M. Pappagallo⁵⁵, L.L. Pappalardo^{19,g}, C. Pappenheimer⁶², W. Parker⁶³, C. Parkes⁵⁹,
 482 G. Passaleva^{20,45}, A. Pastore¹⁷, M. Patel⁵⁸, C. Patrignani^{18,e}, A. Pearce⁴⁵, A. Pellegrino³⁰,
 483 M. Pepe Altarelli⁴⁵, S. Perazzini¹⁸, D. Pereima³⁷, P. Perret⁸, L. Pescatore⁴⁶, K. Petridis⁵¹,
 484 A. Petrolini^{22,h}, A. Petrov⁷³, S. Petrucci⁵⁵, M. Petruzzo^{24,q}, B. Pietrzyk⁷, G. Pietrzyk⁴⁶,
 485 M. Pikiés³², M. Pili⁶⁰, D. Pinci²⁹, J. Pinzino⁴⁵, F. Pisani⁴⁵, A. Piucci¹⁵, V. Placinta³⁵,
 486 S. Playfer⁵⁵, J. Plews⁵⁰, M. Plo Casasus⁴⁴, F. Polci¹¹, M. Poli Lener²¹, M. Poliaková⁶⁵,
 487 A. Poluektov⁹, N. Polukhina^{74,c}, I. Polyakov⁶⁵, E. Polycarpo², G.J. Pomery⁵¹, S. Ponce⁴⁵,
 488 A. Popov⁴², D. Popov⁵⁰, S. Poslavskii⁴², K. Prasanth³², L. Promberger⁴⁵, C. Prouve⁴⁴,
 489 V. Pugatch⁴⁹, A. Puig Navarro⁴⁷, H. Pullen⁶⁰, G. Punzi^{27,p}, W. Qian⁴, J. Qin⁴, R. Quagliani¹¹,
 490 B. Quintana⁸, N.V. Raab¹⁶, R.I. Rabadan Trejo⁹, B. Rachwal³³, J.H. Rademacker⁵¹,
 491 M. Rama²⁷, M. Ramos Pernas⁴⁴, M.S. Rangel², F. Ratnikov^{40,75}, G. Raven³¹, M. Reboud⁷,
 492 F. Redi⁴⁶, F. Reiss¹¹, C. Remon Alepuz⁷⁷, Z. Ren³, V. Renaudin⁶⁰, S. Ricciardi⁵⁴,
 493 S. Richards⁵¹, K. Rinnert⁵⁷, P. Robbe¹⁰, A. Robert¹¹, A.B. Rodrigues⁴⁶, E. Rodrigues⁶²,
 494 J.A. Rodriguez Lopez⁷⁰, M. Roehrken⁴⁵, S. Roiser⁴⁵, A. Rollings⁶⁰, V. Romanovskiy⁴²,
 495 M. Romero Lamas⁴⁴, A. Romero Vidal⁴⁴, J.D. Roth⁷⁸, M. Rotondo²¹, M.S. Rudolph⁶⁵,
 496 T. Ruf⁴⁵, J. Ruiz Vidal⁷⁷, J. Ryzka³³, J.J. Saborido Silva⁴⁴, N. Sagidova³⁶, B. Saitta^{25,f},
 497 C. Sanchez Gras³⁰, C. Sanchez Mayordomo⁷⁷, B. Sanmartin Sedes⁴⁴, R. Santacesaria²⁹,
 498 C. Santamarina Rios⁴⁴, M. Santimaria²¹, E. Santovetti^{28,j}, G. Sarpis⁵⁹, A. Sarti²⁹,
 499 C. Satriano^{29,s}, A. Satta²⁸, M. Saur⁴, D. Savrina^{37,38}, L.G. Scantlebury Smead⁶⁰, S. Schael¹²,
 500 M. Schellenberg¹³, M. Schiller⁵⁶, H. Schindler⁴⁵, M. Schmelling¹⁴, T. Schmelzer¹³, B. Schmidt⁴⁵,
 501 O. Schneider⁴⁶, A. Schopper⁴⁵, H.F. Schreiner⁶², M. Schubiger³⁰, S. Schulte⁴⁶, M.H. Schune¹⁰,
 502 R. Schwemmer⁴⁵, B. Sciascia²¹, A. Sciubba^{29,k}, S. Sellam⁶⁶, A. Semennikov³⁷, A. Sergi^{50,45},
 503 N. Serra⁴⁷, J. Serrano⁹, L. Sestini²⁶, A. Seuthe¹³, P. Seyfert⁴⁵, D.M. Shangase⁷⁸, M. Shapkin⁴²,
 504 T. Shears⁵⁷, L. Shekhtman^{41,x}, V. Shevchenko^{73,74}, E. Shmanin⁷⁴, J.D. Shupperd⁶⁵,
 505 B.G. Siddi¹⁹, R. Silva Coutinho⁴⁷, L. Silva de Oliveira², G. Simi^{26,o}, S. Simone^{17,d}, I. Skiba¹⁹,
 506 N. Skidmore¹⁵, T. Skwarnicki⁶⁵, M.W. Slater⁵⁰, J.G. Smeaton⁵², A. Smetkina³⁷, E. Smith¹²,
 507 I.T. Smith⁵⁵, M. Smith⁵⁸, A. Snoch³⁰, M. Soares¹⁸, L. Soares Lavoura¹, M.D. Sokoloff⁶²,
 508 F.J.P. Soler⁵⁶, B. Souza De Paula², B. Spaan¹³, E. Spadaro Norella^{24,q}, P. Spradlin⁵⁶,
 509 F. Stagni⁴⁵, M. Stahl⁶², S. Stahl⁴⁵, P. Stefko⁴⁶, S. Stefkova⁵⁸, O. Steinkamp⁴⁷, S. Stemmlé¹⁵,
 510 O. Stenyakin⁴², M. Stepanova³⁶, H. Stevens¹³, A. Stocchi¹⁰, S. Stone⁶⁵, S. Stracka²⁷,
 511 M.E. Stramaglia⁴⁶, M. Straticiuc³⁵, S. Strovkov⁷⁶, J. Sun³, L. Sun⁶⁹, Y. Sun⁶³, P. Svihira⁵⁹,
 512 K. Swientek³³, A. Szabelski³⁴, T. Szumlak³³, M. Szymanski⁴, S. Taneja⁵⁹, Z. Tang³,
 513 T. Tekampe¹³, G. Tellarini¹⁹, F. Teubert⁴⁵, E. Thomas⁴⁵, K.A. Thomson⁵⁷, M.J. Tilley⁵⁸,
 514 V. Tisserand⁸, S. T'Jampens⁷, M. Tobin⁵, S. Tolk⁴⁵, L. Tomassetti^{19,g}, D. Tonelli²⁷, D.Y. Tou¹¹,
 515 E. Tournefier⁷, M. Traill⁵⁶, M.T. Tran⁴⁶, C. Trippl⁴⁶, A. Trisovic⁵², A. Tsaregorodtsev⁹,
 516 G. Tuci^{27,45,p}, A. Tully⁴⁶, N. Tuning³⁰, A. Ukleja³⁴, A. Usachov¹⁰, A. Ustyuzhanin^{40,75},
 517 U. Uwer¹⁵, A. Vagner⁷⁶, V. Vagnoni¹⁸, A. Valassi⁴⁵, G. Valenti¹⁸, M. van Beuzekom³⁰,
 518 H. Van Hecke⁶⁴, E. van Herwijnen⁴⁵, C.B. Van Hulse¹⁶, M. van Veghel⁷², R. Vazquez Gomez⁴³,
 519 P. Vazquez Regueiro⁴⁴, C. Vázquez Sierra³⁰, S. Vecchi¹⁹, J.J. Velthuis⁵¹, M. Veltri^{20,r},
 520 A. Venkateswaran⁶⁵, M. Vernet⁸, M. Veronesi³⁰, M. Vesterinen⁵³, J.V. Viana Barbosa⁴⁵,
 521 D. Vieira⁴, M. Vieites Diaz⁴⁶, H. Viemann⁷¹, X. Vilasis-Cardona^{43,m}, A. Vitkovskiy³⁰,
 522 V. Volkov³⁸, A. Vollhardt⁴⁷, D. Vom Bruch¹¹, A. Vorobyev³⁶, V. Vorobyev^{41,x}, N. Voropaev³⁶,
 523 R. Waldi⁷¹, J. Walsh²⁷, J. Wang³, J. Wang⁶⁹, J. Wang⁵, M. Wang³, Y. Wang⁶, Z. Wang⁴⁷,
 524 D.R. Ward⁵², H.M. Wark⁵⁷, N.K. Watson⁵⁰, D. Websdale⁵⁸, A. Weiden⁴⁷, C. Weisser⁶¹,
 525 B.D.C. Westhenry⁵¹, D.J. White⁵⁹, M. Whitehead¹², D. Wiedner¹³, G. Wilkinson⁶⁰,
 526 M. Wilkinson⁶⁵, I. Williams⁵², M. Williams⁶¹, M.R.J. Williams⁵⁹, T. Williams⁵⁰, F.F. Wilson⁵⁴,
 527 M. Winn¹⁰, W. Wislicki³⁴, M. Witek³², G. Wormser¹⁰, S.A. Wotton⁵², H. Wu⁶⁵, K. Wyllie⁴⁵,
 528 Z. Xiang⁴, D. Xiao⁶, Y. Xie⁶, H. Xing⁶⁸, A. Xu³, L. Xu³, M. Xu⁶, Q. Xu⁴, Z. Xu⁷, Z. Xu³,
 529 Z. Yang³, Z. Yang⁶³, Y. Yao⁶⁵, L.E. Yeomans⁵⁷, H. Yin⁶, J. Yu^{6,aa}, X. Yuan⁶⁵,
 530 O. Yushchenko⁴², K.A. Zarebski⁵⁰, M. Zavertyaev^{14,c}, M. Zdybal³², M. Zeng³, D. Zhang⁶,

531 L. Zhang³, S. Zhang³, W.C. Zhang^{3,z}, Y. Zhang⁴⁵, A. Zhelezov¹⁵, Y. Zheng⁴, X. Zhou⁴,
532 Y. Zhou⁴, X. Zhu³, V. Zhukov^{12,38}, J.B. Zonneveld⁵⁵, S. Zucchelli^{18,e}.

533 ¹*Centro Brasileiro de Pesquisas Físicas (CBPF), Rio de Janeiro, Brazil*

534 ²*Universidade Federal do Rio de Janeiro (UFRJ), Rio de Janeiro, Brazil*

535 ³*Center for High Energy Physics, Tsinghua University, Beijing, China*

536 ⁴*University of Chinese Academy of Sciences, Beijing, China*

537 ⁵*Institute Of High Energy Physics (IHEP), Beijing, China*

538 ⁶*Institute of Particle Physics, Central China Normal University, Wuhan, Hubei, China*

539 ⁷*Univ. Grenoble Alpes, Univ. Savoie Mont Blanc, CNRS, IN2P3-LAPP, Annecy, France*

540 ⁸*Université Clermont Auvergne, CNRS/IN2P3, LPC, Clermont-Ferrand, France*

541 ⁹*Aix Marseille Univ, CNRS/IN2P3, CPPM, Marseille, France*

542 ¹⁰*LAL, Univ. Paris-Sud, CNRS/IN2P3, Université Paris-Saclay, Orsay, France*

543 ¹¹*LPNHE, Sorbonne Université, Paris Diderot Sorbonne Paris Cité, CNRS/IN2P3, Paris, France*

544 ¹²*I. Physikalisches Institut, RWTH Aachen University, Aachen, Germany*

545 ¹³*Fakultät Physik, Technische Universität Dortmund, Dortmund, Germany*

546 ¹⁴*Max-Planck-Institut für Kernphysik (MPIK), Heidelberg, Germany*

547 ¹⁵*Physikalisches Institut, Ruprecht-Karls-Universität Heidelberg, Heidelberg, Germany*

548 ¹⁶*School of Physics, University College Dublin, Dublin, Ireland*

549 ¹⁷*INFN Sezione di Bari, Bari, Italy*

550 ¹⁸*INFN Sezione di Bologna, Bologna, Italy*

551 ¹⁹*INFN Sezione di Ferrara, Ferrara, Italy*

552 ²⁰*INFN Sezione di Firenze, Firenze, Italy*

553 ²¹*INFN Laboratori Nazionali di Frascati, Frascati, Italy*

554 ²²*INFN Sezione di Genova, Genova, Italy*

555 ²³*INFN Sezione di Milano-Bicocca, Milano, Italy*

556 ²⁴*INFN Sezione di Milano, Milano, Italy*

557 ²⁵*INFN Sezione di Cagliari, Monserrato, Italy*

558 ²⁶*INFN Sezione di Padova, Padova, Italy*

559 ²⁷*INFN Sezione di Pisa, Pisa, Italy*

560 ²⁸*INFN Sezione di Roma Tor Vergata, Roma, Italy*

561 ²⁹*INFN Sezione di Roma La Sapienza, Roma, Italy*

562 ³⁰*Nikhef National Institute for Subatomic Physics, Amsterdam, Netherlands*

563 ³¹*Nikhef National Institute for Subatomic Physics and VU University Amsterdam, Amsterdam,
564 Netherlands*

565 ³²*Henryk Niewodniczanski Institute of Nuclear Physics Polish Academy of Sciences, Kraków, Poland*

566 ³³*AGH - University of Science and Technology, Faculty of Physics and Applied Computer Science,
567 Kraków, Poland*

568 ³⁴*National Center for Nuclear Research (NCBJ), Warsaw, Poland*

569 ³⁵*Horia Hulubei National Institute of Physics and Nuclear Engineering, Bucharest-Magurele, Romania*

570 ³⁶*Petersburg Nuclear Physics Institute NRC Kurchatov Institute (PNPI NRC KI), Gatchina, Russia*

571 ³⁷*Institute of Theoretical and Experimental Physics NRC Kurchatov Institute (ITEP NRC KI), Moscow,
572 Russia, Moscow, Russia*

573 ³⁸*Institute of Nuclear Physics, Moscow State University (SINP MSU), Moscow, Russia*

574 ³⁹*Institute for Nuclear Research of the Russian Academy of Sciences (INR RAS), Moscow, Russia*

575 ⁴⁰*Yandex School of Data Analysis, Moscow, Russia*

576 ⁴¹*Budker Institute of Nuclear Physics (SB RAS), Novosibirsk, Russia*

577 ⁴²*Institute for High Energy Physics NRC Kurchatov Institute (IHEP NRC KI), Protvino, Russia,
578 Protvino, Russia*

579 ⁴³*ICCUB, Universitat de Barcelona, Barcelona, Spain*

580 ⁴⁴*Instituto Galego de Física de Altas Enerxías (IGFAE), Universidade de Santiago de Compostela,
581 Santiago de Compostela, Spain*

582 ⁴⁵*European Organization for Nuclear Research (CERN), Geneva, Switzerland*

583 ⁴⁶*Institute of Physics, Ecole Polytechnique Fédérale de Lausanne (EPFL), Lausanne, Switzerland*

584 ⁴⁷*Physik-Institut, Universität Zürich, Zürich, Switzerland*

585 ⁴⁸*NSC Kharkiv Institute of Physics and Technology (NSC KIPT), Kharkiv, Ukraine*

586 ⁴⁹*Institute for Nuclear Research of the National Academy of Sciences (KINR), Kyiv, Ukraine*

587 ⁵⁰ *University of Birmingham, Birmingham, United Kingdom*
588 ⁵¹ *H.H. Wills Physics Laboratory, University of Bristol, Bristol, United Kingdom*
589 ⁵² *Cavendish Laboratory, University of Cambridge, Cambridge, United Kingdom*
590 ⁵³ *Department of Physics, University of Warwick, Coventry, United Kingdom*
591 ⁵⁴ *STFC Rutherford Appleton Laboratory, Didcot, United Kingdom*
592 ⁵⁵ *School of Physics and Astronomy, University of Edinburgh, Edinburgh, United Kingdom*
593 ⁵⁶ *School of Physics and Astronomy, University of Glasgow, Glasgow, United Kingdom*
594 ⁵⁷ *Oliver Lodge Laboratory, University of Liverpool, Liverpool, United Kingdom*
595 ⁵⁸ *Imperial College London, London, United Kingdom*
596 ⁵⁹ *Department of Physics and Astronomy, University of Manchester, Manchester, United Kingdom*
597 ⁶⁰ *Department of Physics, University of Oxford, Oxford, United Kingdom*
598 ⁶¹ *Massachusetts Institute of Technology, Cambridge, MA, United States*
599 ⁶² *University of Cincinnati, Cincinnati, OH, United States*
600 ⁶³ *University of Maryland, College Park, MD, United States*
601 ⁶⁴ *Los Alamos National Laboratory (LANL), Los Alamos, United States*
602 ⁶⁵ *Syracuse University, Syracuse, NY, United States*
603 ⁶⁶ *Laboratory of Mathematical and Subatomic Physics , Constantine, Algeria, associated to ²*
604 ⁶⁷ *Pontificia Universidade Católica do Rio de Janeiro (PUC-Rio), Rio de Janeiro, Brazil, associated to ²*
605 ⁶⁸ *South China Normal University, Guangzhou, China, associated to ³*
606 ⁶⁹ *School of Physics and Technology, Wuhan University, Wuhan, China, associated to ³*
607 ⁷⁰ *Departamento de Física , Universidad Nacional de Colombia, Bogota, Colombia, associated to ¹¹*
608 ⁷¹ *Institut für Physik, Universität Rostock, Rostock, Germany, associated to ¹⁵*
609 ⁷² *Van Swinderen Institute, University of Groningen, Groningen, Netherlands, associated to ³⁰*
610 ⁷³ *National Research Centre Kurchatov Institute, Moscow, Russia, associated to ³⁷*
611 ⁷⁴ *National University of Science and Technology “MISIS”, Moscow, Russia, associated to ³⁷*
612 ⁷⁵ *National Research University Higher School of Economics, Moscow, Russia, associated to ⁴⁰*
613 ⁷⁶ *National Research Tomsk Polytechnic University, Tomsk, Russia, associated to ³⁷*
614 ⁷⁷ *Instituto de Física Corpuscular, Centro Mixto Universidad de Valencia - CSIC, Valencia, Spain,*
615 *associated to ⁴³*
616 ⁷⁸ *University of Michigan, Ann Arbor, United States, associated to ⁶⁵*

617 ^a *Universidade Federal do Triângulo Mineiro (UFMT), Uberaba-MG, Brazil*
618 ^b *Laboratoire Leprince-Ringuet, Palaiseau, France*
619 ^c *P.N. Lebedev Physical Institute, Russian Academy of Science (LPI RAS), Moscow, Russia*
620 ^d *Università di Bari, Bari, Italy*
621 ^e *Università di Bologna, Bologna, Italy*
622 ^f *Università di Cagliari, Cagliari, Italy*
623 ^g *Università di Ferrara, Ferrara, Italy*
624 ^h *Università di Genova, Genova, Italy*
625 ⁱ *Università di Milano Bicocca, Milano, Italy*
626 ^j *Università di Roma Tor Vergata, Roma, Italy*
627 ^k *Università di Roma La Sapienza, Roma, Italy*
628 ^l *AGH - University of Science and Technology, Faculty of Computer Science, Electronics and*
629 *Telecommunications, Kraków, Poland*
630 ^m *LIFAELS, La Salle, Universitat Ramon Llull, Barcelona, Spain*
631 ⁿ *Hanoi University of Science, Hanoi, Vietnam*
632 ^o *Università di Padova, Padova, Italy*
633 ^p *Università di Pisa, Pisa, Italy*
634 ^q *Università degli Studi di Milano, Milano, Italy*
635 ^r *Università di Urbino, Urbino, Italy*
636 ^s *Università della Basilicata, Potenza, Italy*
637 ^t *Scuola Normale Superiore, Pisa, Italy*
638 ^u *Università di Modena e Reggio Emilia, Modena, Italy*
639 ^v *Università di Siena, Siena, Italy*
640 ^w *MSU - Iligan Institute of Technology (MSU-IIT), Iligan, Philippines*
641 ^x *Novosibirsk State University, Novosibirsk, Russia*
642 ^y *Sezione INFN di Trieste, Trieste, Italy*

643 ^z*School of Physics and Information Technology, Shaanxi Normal University (SNNU), Xi'an, China*

644 ^{aa}*Physics and Micro Electronic College, Hunan University, Changsha City, China*

645 [†]*Deceased*